Tuning of localized surface plasmon resonance of well-ordered Ag/Au bimetallic nanodot arrays by laser interference lithography and thermal annealing

Le Xu,[1,2] Leng Seow Tan,[2] and Ming Hui Hong[1,2,*]

[1]Department of Electrical and Computer Engineering, National University of Singapore, 4 Engineering Drive 3, Singapore 117576

[2]Data Storage Institute, Agency for Science, Technology and Research, DSI Building, 5 Engineering Drive 1, Singapore 117608

*Corresponding author: elehmh@nus.edu.sg

Received 1 July 2011; revised 5 September 2011; accepted 9 September 2011; posted 12 September 2011 (Doc. ID 150273); published 14 October 2011

A novel hybrid approach to fabricate large-area well-ordered Ag/Au bimetallic nanodot arrays and its potential applications for biosensing is investigated. With the combination of laser interference lithography and the thermal annealing technique, Ag/Au bimetallic nanodots about ~50 nm are formed inside periodic nanodisk arrays at a dimension of ~530 nm on quartz substrates. Extinction spectra of the fabricated nanostructures show their localized surface plasmon resonance (LSPR) can be well controlled by Au concentration, which offers a means to flexibly tune the optical properties of the nanodot arrays. To study the sensitivity of the nanodot arrays, resonance wavelength changes per refractive index unit (RIU) are performed in different surrounding environments. This shows a 94% increase in peak shift per refractive index unit (nanometers/RIU) compared to the nanodot arrays formed only by thermal annealing. These results demonstrate a feasible approach to improve LSPR-based biosensor performance.

OCIS codes: 220.3740, 310.6628, 240.6680.

1. Introduction

Localized surface plasmon resonance (LSPR) is an attractive nanoscale research area. LSPR occurs when metallic nanostructures are illuminated by a specific wavelength of light and the excitation of surface plasmons is localized within nanoparticles [1]. These resonances, associated with noble metal nanostructures, create sharp spectral absorption and scattering peaks as well as strong electromagnetic near-field enhancements [2], which are widely applied to a variety of applications in biosensing [3], solar cells [4], surface enhanced spectroscopy [5], near-field scanning optical microscopy [6], and optical switching [7]. Among these, the LSPR biosensing technique can create a label-free biosensor by monitoring the LSPR peak shifts from molecular interactions near the nanoparticle surface [1,2]. These sensors are beneficial from the merits of simple and low-cost measurement, easily performed in a transmission spectrum mode with high sensitivity in a small detection sensor [8]. The LSPR resonance wavelength strongly depends on not only the material and geometry of nanostructures but also the refractive index of the surrounding media. Therefore, understanding how these nanostructures influence LSPR properties, optimize the nanostructures' design, and improve their detection sensitivity are important issues for LSPR-based biosensor research.

0003-6935/11/310G74-06$15.00/0

In order to further practice these applications, the synthesis and assembly of functional surface-immobilized nanostructure arrays are investigated with desirable features, such as low-cost fabrication, large-area nanopatterning, reproducibility, and tunability of their optical properties. Therefore, a traditional approach to form these nanostructures is to transform chemically synthesized nanoparticles [9] from suspensions to solid substrates, so as to obtain the LSPR properties from an ensemble of nanoparticles. This method can be applied to the precise control of the size and shape of the metallic nanoparticles by modifying parameters, but has a critical technical issue on how to fabricate nanoparticles with well-controllable interparticle space over a large area (in centimeter scale and regular periodic arrays). An alternative method for low-cost nanopatterning, such as nanosphere lithography [10], has been used in the fabrication of metallic nanostructures. However, this method is hard to lift off and difficult to assemble into monolayer nanospheres at a diameter of ~50 nm. In this paper, we present a novel hybrid and low-cost approach to fabricate large-area well-ordered Ag/Au bimetallic nanodot arrays by the combination of laser interference lithography (LIL) and thermal annealing. LIL, as a large-area, maskless, and noncontact nanofabrication technique, can be applied to make periodic nanolines and nanodisks on metallic thin films in a short time (only a few minutes exposure) [11], but the dimension of the nanostructures is of the submicrometer scale. Thermal annealing of continuous metallic thin films, also known as the dewetting process, provides a simple means to fabricate large-area nanostructures at a particle size of ~50 nm, but cannot form well-ordered nanostructures. With the combination of the LIL and thermal annealing, Ag/Au bimetallic nanodot arrays at a particle size of ~50 nm can be formed inside periodic nanodisk arrays on a quartz substrate. To investigate the LSPR of the fabricated nanodot arrays, extinction spectra are measured by micro-UV-visible spectrometer, which shows the blueshift peak position, a narrow FWHM, and increasing intensity of the LSPR. The tunability of the LSPR peak position can be achieved by the variation of Au concentration, which can be controlled by the thickness of the Ag/Au bimetallic thin films during the metal deposition. To study the sensitivity of the nanodot arrays, resonance wavelength change per refractive index unit (RIU) is performed in different surrounding environments. It indicates a 94% increase in peak shift per refractive index unit (nanometers/RIU) compared to nanodots fabricated only by thermal annealing. These results demonstrate a feasible approach to improve LSPR-based biosensor performance.

2. Experimental

The fabrication process of the Ag/Au nanodot arrays on a quartz substrate is schematically illustrated in Fig. 1. It includes photoresist (PR) spin coating, PR exposure by LIL, PR developing, reactive ion etching (RIE), metal deposition, lift-off, and thermal annealing. First, in order to remove contaminants, the quartz substrate at a dimension of 15 mm × 15 mm × 0.4 mm is exposed to solutions of acetone, isopropyl alcohol, and deionized water in an ultrasonic bath for 30 min each. A spin coater is used to coat negative PR (N1405, Micro Resist Technology) on top of the substrate at 500 rpm for 10 s and then 5000 rpm for 50 s. After soft baking for 60 s, these samples are exposed by a 325 nm helium–cadmium (He–Cd) continuous wave laser (Lloyd's mirror setup) [12]. Nanodisk arrays are made by double exposure, with one 90° rotation of the sample for the second exposure. PR developing is done by immersing the sample in the developer for 18 s. The developer dissolves the negative photoresist that is not exposed by the laser. Anisotropic RIE (Oxford Instruments) is applied to remove unexposed PR. Metallic thin films are deposited by an electron beam evaporation system (BOC Edwards ED03) at room temperature and lift-off. On the bottom of the layer is 1 nm Cr to increase the adhesion between the Ag/Au bimetallic thin films and the

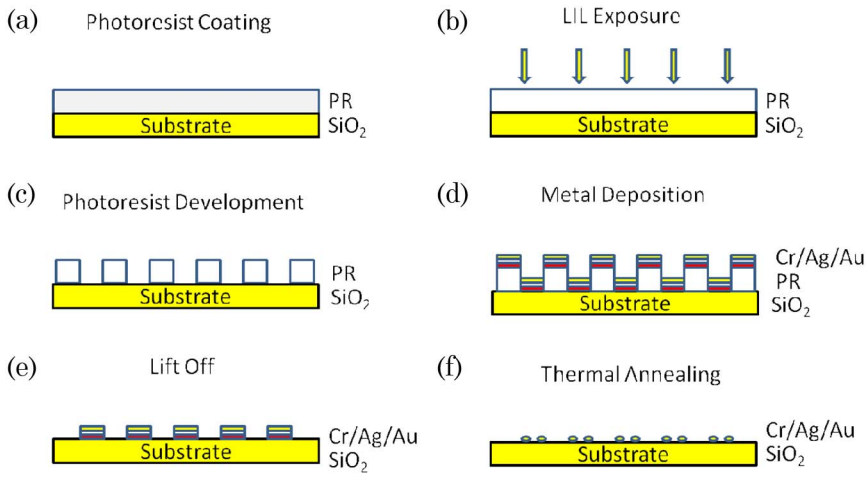

Fig. 1. (Color online) Fabrication of Ag/Au bimetallic nanodots arrays by LIL and thermal annealing: (a) PR spin coating; (b) PR exposure by LIL; (c) PR developing; (d) Cr, Ag, and Au metallic thin film deposition; (e) lift-off; and (f) thermal annealing.

quartz substrate. Ag and Au thin films are deposited sequentially on top of the Cr thin film. The total thickness of the bimetallic Ag/Au thin films is set as a constant of 8 nm. The Au concentration of the Ag_{1-x}/Au_x bimetallic thin films is varied by adjusting the thickness of the Au thin film. After the metal deposition, PG remover (MicroChem Corp.) is used to lift off the PR, leaving only the metal films deposited on the substrate. The lift-off is performed in an ultrasonic bath for 20 min at 70 °C. Finally, thermal annealing is carried out in a high-temperature furnace (Nabertherm HTCT 01/14) at 500 °C for 4 h at a heating rate of 25 °C/ min and the samples are cooled to room temperature. The extinction (absorption and scattering) spectra of the nanodot arrays are measured by using a micro-UV-visible spectrophotometer at normal incidence in transmission mode. The morphology of the fabricated nanostructures is analyzed by a scanning electron microscope (SEM, FE SEM 7401F). To measure the sensitivity of the nanostructures, the resonance peak shift induced by refractive index change is measured in air, methanol, and ethanol ($n = 1$, 1.3290, and 1.3614) [13].

3. Results and Discussion

Figure 2 shows SEM images of $Ag_{0.75}/Au_{0.25}$ bimetallic nanodisk arrays made by LIL (a) before and (b) after the thermal annealing on quartz substrates, as well as the extinction spectra measured in the transmission mode. The Au concentration of $Ag_{0.75}/Au_{0.25}$ nanodisk arrays is achieved by controlling the thickness of Ag/Au thin films as 6/2 nm during the metal deposition. Before the thermal annealing, it is observed that $Ag_{0.75}/Au_{0.25}$ bimetallic nanodisk arrays at a diameter of 538 ± 18 nm are formed at a period of ~930 nm on the quartz substrate. The structure exhibits excellent large-area uniformity over an area of 8 mm × 8 mm. After the thermal annealing at 500 °C for 4 h, the $Ag_{0.75}/Au_{0.25}$ bimetallic nanodisk arrays are heated above the melting temperature, so the surfaces of Ag/Au thin films begin to fluctuate and then deform by the squeezing mode, in which the two perturbations between the Ag/Au and Ag/SiO_2 interfaces are completely out of phase with each other. The alloy nanodots are self-organized due to an instability arising when the stabilizing surface tension force is overcome by destabilizing attractive intermolecular dispersion forces [14]. The extinction spectra of the nanodot arrays are measured in transmission mode by unpolarized light in air. There is only one resonance peak in the LSPR band of the nanodot arrays, which indicates alloy nanostructures are formed instead of the Ag/Au core/shell nanostructures [15]. As can be seen from Fig. 2(c), the nanodisk arrays before the thermal annealing exhibit a broad LSPR band with the resonance peak at 872 nm, while the annealed nanodisk arrays show an intense and narrow extinction spectrum with the LSPR peak at 508 nm. Meanwhile, the FWHM of the LSPR band reduces from 170 to 63 nm and the peak position blueshifts from 872 to 508 nm. According

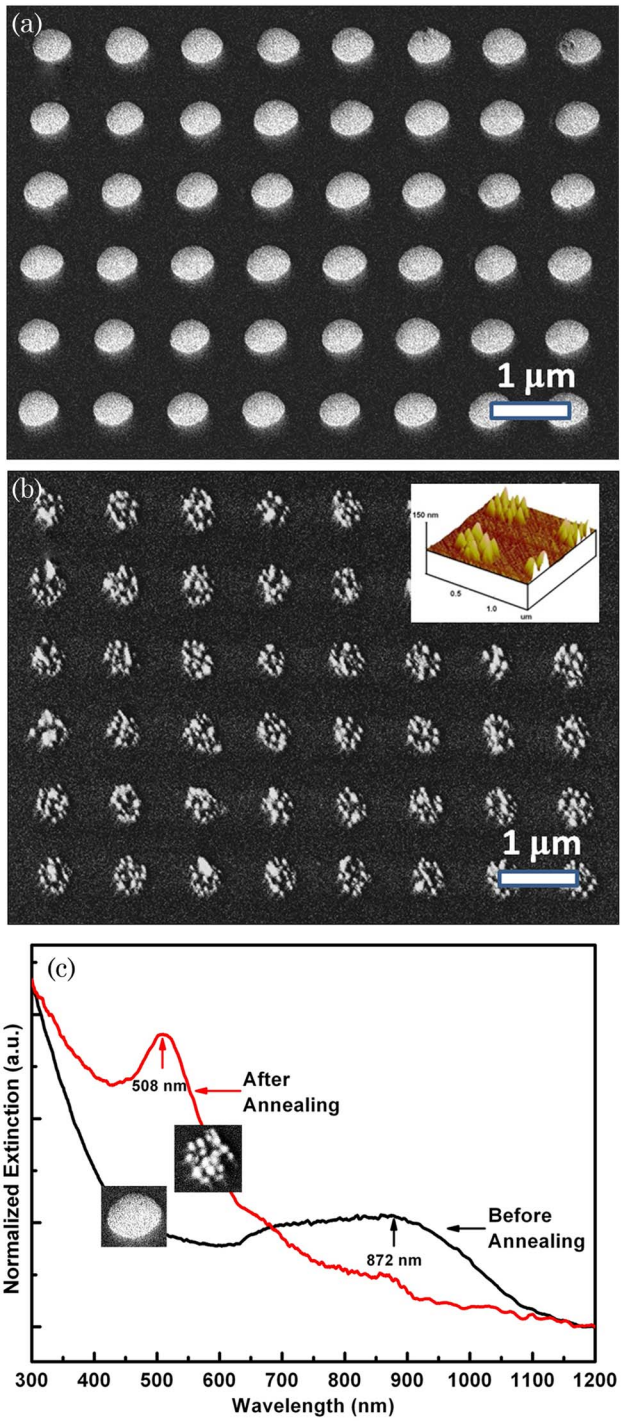

Fig. 2. (Color online) SEM images of $Ag_{0.75}/Au_{0.25}$ bimetallic nanodisk arrays fabricated by LIL (a) before and (b) after thermal annealing, and (c) their measured extinction spectra.

to the previous works [16,17], the FWHM, peak position, and intensity of LSPR strongly depend on the size, shape, distribution, and material of the nanostructures, as well as their surrounding environment. The observed behaviors of the LSPR in the $Ag_{0.75}/Au_{0.25}$ nanodisk arrays before and after thermal annealing are attributed to three key factors: interparticle distance and the size and shape of the nanodot arrays. After thermal annealing, the

diameter of the nanodisk decreases 10 times from 538 ± 18 to 50 ± 30 nm, and the height of the nanodisk increases from 8 ± 2 to 45 ± 15 nm, respectively, as analyzed by the SEM image of the nanodot arrays [Fig. 2(b)]. The shape of the nanodisk becomes spheroid. Furthermore, the resonance wavelength, the FWHM, and the extinction intensity of the nanostructure are also influenced by the interparticle distance. Before thermal annealing, the nanodisk arrays at a diameter of 538 ± 18 nm show a long resonance wavelength, a broad FWHM, and low intensity due to the large interparticle distance among the nanodisks, which results in strong radiative dipolar interaction (far-field coupling) [15]. After thermal annealing, the nanodisk was ruptured into many nanodots with 45 ± 15 nm interparticle distances among the nanodots. The interparticle distance of the nanodisk arrays, however, is not changed during the thermal dewetting process because the periodic distance ($p = \lambda/2 \sin\theta$) is determined by the angle of two interference beams (2θ) and the wavelength of the laser source (λ), which are fixed by the LIL process. The resonance wavelength of the nanodot arrays decreases greatly mainly due to the smaller interparticle distance among nanodots into the nanodisks, leading to the strong near-field coupling. The dipolar coupling among the nanodots contributes to the change for the optical properties of LSPR. Therefore, after thermal annealing, the nanodot arrays of spheroid shape, small size (50 ± 30 nm), and interparticle spacing (45 ± 15 nm) exhibit a 364 nm blueshift of the LSPR peak position and a 107 nm decrease of the FWHM.

Figure 3 shows the extinction spectra of the nanodot arrays at different Au concentrations. It is observed that the LSPR peak of the $Ag_{0.75}/Au_{0.25}$ nanodot arrays is at 508 nm, while $Ag_{0.5}/Au_{0.5}$ nanodot arrays show a LSPR peak at 528 nm due to the increase of Au concentration. The Au concentration can be well controlled by the metal thin film deposition. 6/2 and 4/4 nm of Ag/Au thin films are coated on 1 nm Cr thin films. Both nanodisk arrays are annealed at 500 °C for 4 h at the same time. It is observed that there is a 20 nm redshift of the LSPR peak position as the Au thickness increases from 2 to 4 nm after thermal annealing. Meanwhile, the effect of the adhesion layer on the fabricated nanostructures can lead to a minor blueshift of the peak position and broader linewidth due to the refractive index change. However, since the Cr thin film is 1 nm for all the samples in our experiments, we focus our research efforts on the peak shift (difference) due to the variation of Au concentration. In this paper, we neglected the 1 nm Cr thin film influence on the peak shift. According to the Mie theory [16], the extinction cross section can be determined by the effective dielectric constants and surrounding media as well as the concentration of the metal particles, while the effective dielectric constant of the alloy nanodot arrays varies with the bulk dielectric constant of Au, which can be well defined by the close-to-linear correlation between the wavelength shift of the LSPR extinction maximum and the composition of the nanostructure. In the case of Ag_{1-x}/Au_x alloy, the effective dielectric constant can be estimated from $\varepsilon(x,\omega)_{Ag_{1-x}Au_x} = (1-x)\varepsilon(\omega)_{Ag} + x\varepsilon(\omega)_{Au}$ [18]. The plasma frequency of the alloy is not much different from that of the parent metals considering the d-band transition effect on the effective dielectric function of the Ag/Au alloy. This is due to the gradual change in the d-band structure of the alloy with change in Ag/Au composition and its effect on the composition of the dielectric function [19]. Therefore, the LSPR resonance wavelength shifts to the longer wavelength as Au concentration increases. It is clearly indicated that there is a 20 nm redshift of the LSPR peak as the Au concentration increases. This offers a flexible means to tune the LSPR peak based on the Au concentration, which extends the applications for LSPR biosensors.

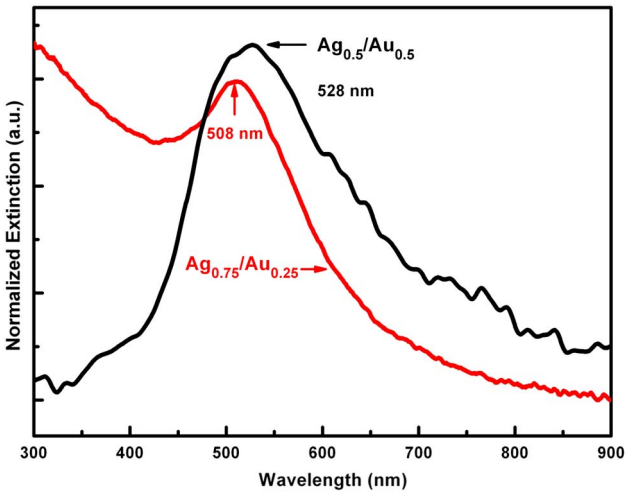

Fig. 3. (Color online) Extinction spectra of bimetallic Ag/Au nanodisk arrays formed by the combination of LIL and thermal annealing at different Au concentrations.

To analyze the sensing characteristics of the $Ag_{0.75}/Au_{0.25}$ nanodot arrays on quartz substrates as an LSPR-based sensor, extinction spectra at different environments were measured, as shown in Fig. 4(a). It is observed that the LSPR peak positions in air, methanol, and ethanol redshift from 508 to 529 and 532 nm. The redshift peak is due to the increases of refractive index in the surrounding environments from 1 to 1.3290 to 1.3614 [13]. According to Mie theory [16], the location of the extinction maximum of the noble metal nanoparticles is highly dependent on the dielectric properties of the surrounding environments. The wavelength shift in the extinction maximum of nanoparticles can be used to detect the properties of the molecules surrounding the nanoparticles. The sensitivity of the nanostructures are experimentally determined by the slope of a linear fit in the plot of LSPR peak wavelength versus the refractive index, as shown in Fig. 4(b). As a reference, the nanodots are formed by the thermal annealing of Ag/Au bimetallic thin films (6/2 nm) at 500 °C for 4 h.

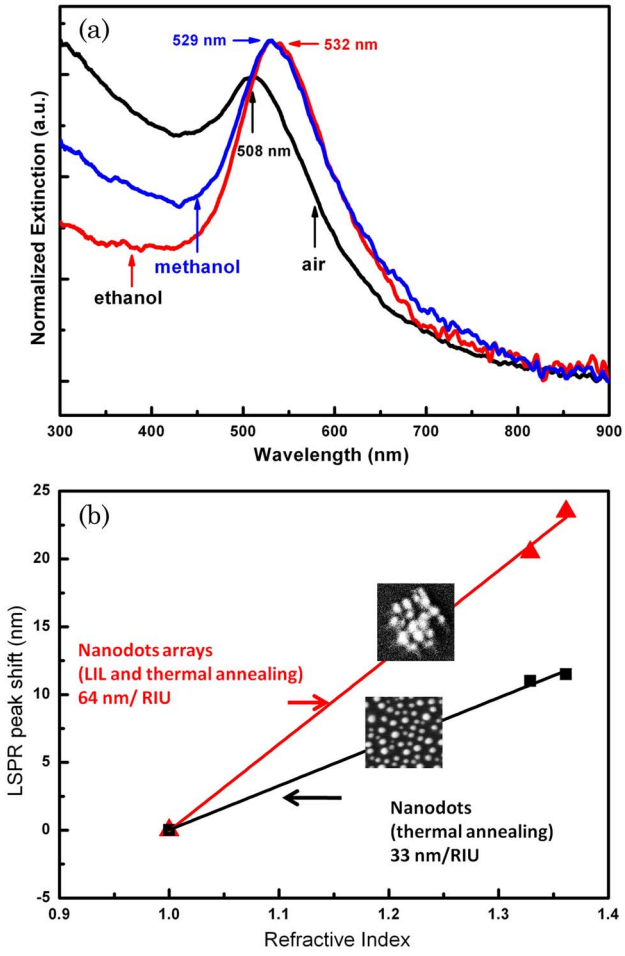

Fig. 4. (Color online) (a) Experimental extinction spectra of the $Ag_{0.75}/Au_{0.25}$ nanodot arrays in different environments: air, methanol, and ethanol ($n = 1$, 1.3290, and 1.3614), and (b) peak shift of the $Ag_{0.75}/Au_{0.25}$ nanodot arrays in different environments.

The LSPR peak shift per refractive index of the nanodot arrays is 64 nm/RIU for LIL and thermal annealing, which is 94% higher than the nanodots formed by thermal annealing only. This shows that the nanostructure fabricated by the combination of the LIL and thermal annealing can improve the performance of LSPR sensing.

4. Conclusions

With the combination of LIL and thermal annealing, Ag/Au bimetallic nanodot arrays at a particle size of ~50 nm can be formed inside periodic nanodisk arrays at a dimension of ~530 nm on quartz substrate. To investigate the LSPR behaviors of the fabricated nanodot arrays, extinction spectra are measured by a micro-UV-visible spectrometer. It shows that bimetallic nanodot arrays are formed, resulting in a dramatic blueshift of the resonance peak, narrower FWHM, and higher intensity of the LSPR. This is because the smaller diameter, spheroid shape, and narrower interparticle spacing of the nanodot arrays are formed by LIL and thermal annealing. The tunability of the LSPR peak position can be achieved by the variation of Au concentration, which can be simply tuned by metallic thin film deposition. To further study the sensitivity of nanodot arrays in biosensing applications, the peak shift versus refractive index measurements are performed in different surrounding environments. A 94% increase in the peak shift per refractive index unit (nanometers/RIU) is observed compared to the nanodots fabricated by thermal annealing only. These results demonstrate a hybrid approach to improve LSPR-based biosensor performance.

The authors acknowledge funding provided by the Agency for Science, Technology And Research/Science and Engineering Research Council (ASTAR/SERC) Superlens Program (Project No. 092 154 0099) for the research work published in this paper.

References

1. Y. B. Zheng, L. Jensen, W. Yan, and T. R. Walker, B. K. Juluri, L. Jensen, and T. J. Huang, "Chemically tuning the localized surface plasmon resonances of gold nanostructure arrays," J. Phys. Chem. C **113**, 7019–7024 (2009).
2. K. M. Mayer and J. H. Hafner, "Localized surface plasmon resonance sensors," Chem. Rev. **111**, 3828–3857 (2011).
3. A. D. Van McFarland and R. P. Duyne, "Single silver nanoparticles as real-time optical sensors with zeptomole sensitivity," Nano Lett. **3**, 1057–1062 (2003).
4. K. R. Catchpole and A. Polman, "Plasmonic solar cells," Opt. Express **16**, 21793–21800 (2008).
5. Y. Hou, J. Xu, P. Wang, and D. Yu, "Surface-enhanced Raman spectroscopy on coupled two-layer nanorings," Appl. Phys. Lett. **96**, 203107 (2010).
6. R. Esteban, R. Vogelgesang, J. Dorfmuller, A. Dmitriev, C. Rockstuhl, C. Etrich, and K. Kern, "Direct near-field optical imaging of higher order plasmonic resonances," Nano Lett. **8**, 3155–3159 (2008).
7. V. K. S. Hsiao, Y. B. Zheng, B. K. Juluri, and T. J. Huang, "Light-driven plasmonic switches based on Au nanodisk arrays and photoresponsive liquid crystals," Adv. Mater. **20**, 3528–3532 (2008).
8. J. N. Anker, W. P. Hall, O. Lyandres, N. C. Shah, J. Zhao, and R. P. Van Duyne, "Biosensing with plasmonic nanosensors," Nat. Mater. **7**, 442–453 (2008).
9. G. Raschke, S. Kowarik, T. Franzl, C. Sonnichsen, T. A. Klar, and J. Feldmann, "Biomolecular recognition based on single gold nanoparticle light scattering," Nano Lett. **3**, 935–938 (2003).
10. A. J. Haes and R. P. Van Duyne, "A nanoscale optical biosensor: sensitivity and selectivity of an approach based on the localized surface plasmon resonance spectroscopy of triangular silver nanoparticles," J. Am. Chem. Soc. **124**, 10596–10604 (2002).
11. C. H. Liu, M. H. Hong, H. W. Cheung, F. Zhang, Z. Q. Huang, L. S. Tan, and T. S. A. Hor, "Bimetallic structure fabricated by laser interference lithography for tuning surface plasmon resonance," Opt. Express **16**, 10701–10709 (2008).
12. M. L. Schattenburg, R. J. Aucoin, and R. C. Fleming, "Optically matched trilevel resist process for nanostructure fabrication," J. Vac. Sci. Technol. B **13**, 3007–3011 (1995).
13. D. R. Lide, *Handbook of Chemistry and Physics*, 87th ed. (CRC Press, 2006).

14. H. Krishna, N. Shirato, S. Yadavali, R. Sachan, J. Strader, and R. Kalyanaraman, "Self-organization of nanoscle multilayer liquid metal films: experiment and theory," ACS Nano **5**, 470–476 (2011).
15. N. E. Motl, E. Ewusi-Ann, I. T. Sines, L. Jensen, and R. E. Schaak, "Au-Cu alloy nanoparticles with tunable compositions and plasmonic properties: experimental determination of composition and correlation with theory," J. Phys. Chem. C **114**, 19263–19269 (2010).
16. K. L. Kelly and G. C. Schatz, "The optical properties of metal nanoparticles: the influence of size, shape, and dielectric environment," J. Phys. Chem. B **107**, 668–677 (2003).
17. T. Sannomiya, P. K. Sahoo, D. I. Mahcicek, H. H. Solak, C. Hafner, D. Grieshaber, and J. Voros, "Biosensing by densely packed and optically coupled plasmonic particle arrays," Small **5**, 1889–1896 (2009).
18. R. K. Roy, S. K. Mandal, and A. K. Pal, "Effect of interfacial alloying on the surface plasmon resonance of nanocrystalline Au-Ag multilayer thin films," Eur. Phys. J. B **33**, 109–114 (2003).
19. Y. B. Zheng, B. K. Juluri, X. Mao, T. R. Walker, and T. J. Huang, "Systematic investigation of localized surface plasmon resonance of long range ordered Au nanodisk arrays," J. Appl. Phys. **103**, 014308 (2008).